

bradscholars

Interfacial cocrystallization using oily phase via liquid–liquid phase separation

Item Type	Article
Authors	Sajid, Asim;Alsirawan, MHD Bashir;Seaton, Colin C.;Swift, Thomas;Pagire, Sudhir K.;Vangala, Venu R.;Kelly, Adrian L.;Paradkar, Anant R
Citation	Al-Hanafi Sajid A, Alsirawan MHDB, Seaton CC et al (2022) Interfacial cocrystallization using oily phase via liquid–liquid phase separation. <i>Crystal, Growth & Design</i> . 22(10): 5845-5851.
DOI	https://doi.org/10.1021/acs.cgd.2c00263
Rights	© 2022 The Authors. Published by American Chemical Society. This work is licensed under a Creative Commons Attribution 4.0 International License. http://creativecommons.org/licenses/by/4.0/
Download date	2026-04-12 13:18:32
Link to Item	https://bradscholars.brad.ac.uk/handle/10454/19177.2

Interfacial Cocrystallization Using Oily Phase via Liquid–Liquid Phase Separation

Published as part of a *Crystal Growth & Design* joint virtual special issue on *Crystallizing the Role of Solid-State Form in Drug Delivery*

M. Asim Sajid Al-Hanafy, Mhd Bashir Alsirawan, Colin C. Seaton, Thomas Swift, Sudhir Pagire, Venu R. Vangala, Adrian L. Kelly, and Anant Paradkar*



Cite This: *Cryst. Growth Des.* 2022, 22, 5845–5851



Read Online

ACCESS |



Metrics & More

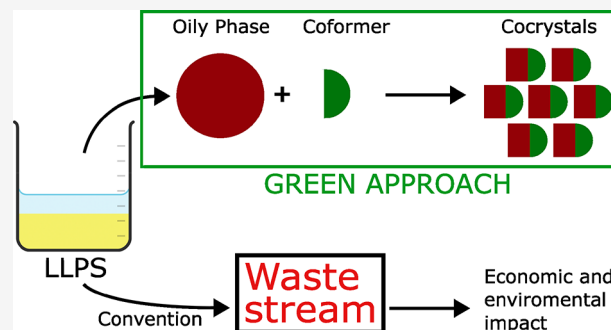


Article Recommendations



Supporting Information

ABSTRACT: Cocrystals consist of two molecules bonded together in a single crystal lattice giving rise to wide applications including improving solubility of poorly soluble pharmaceuticals. Cocrystallization reaction occurs in the oily phase of liquid–liquid phase separation (LLPS) after it is mixed with coformers. Indomethacin–saccharin cocrystal formation was monitored *in situ*, and the kinetics of crystallization were determined. The crystallization rates show that the process can be proposed to prevent unwanted oily phase formation during LLPS.



INTRODUCTION

Liquid–liquid phase separation (LLPS), also known as oiling out/demixing, is a commonly occurring phenomenon during the antisolvent mediated crystallization process which is a crucial step during active ingredient synthesis. LLPS is known to be a problematic event as it can halt or slow down the intended crystallization process. Moreover, crystals produced along LLPS do not have the desired physicochemical properties. Crystallization in systems that undergo LLPS have been reported to produce crystals with higher impurities that easily agglomerate.¹ Moreover, oiling out can coat processing equipment and render batches of the product unusable.² LLPS can significantly delay the development process, with discarded batches presenting downstream challenges including disposal of precious active materials, and promote sustainable manufacturing. Although LLPS is recognized as a deleterious process, it is intentionally performed for certain applications such as the formation of spherical particles, the formation of metastable polymorphs, and the separation of fatty acids, proteins, and polymers. Normally, during solvent–antisolvent mediated crystallization, the antisolvent would have more affinity toward the solvent compared to the solute. This makes the solvent less available to the solute, forming a supersaturated solution leading to solute crystallization, known as solid–liquid phase separation (SLPS).³ In certain cases, LLPS occurs instead of SLPS as the supersaturated solution separates into two liquid phases: a solute-abundant phase and a solvent-abundant phase. The solute-abundant phase contains highly concentrated solute in the form of a viscous oil-

like phase, while the solvent-abundant phase is a clear low viscous liquid. However, solute molecules can be found in both phases at different concentrations.^{4,5}

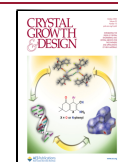
The mechanism of LLPS is not fully established. However, reports suggested that LLPS occurs when high levels of supersaturation are achieved and the crystal growth rate of the solute is slow enough that it is almost hindered by the high viscosity of the supersaturated solution.^{4,5} LLPS is enthalpy driven and occurs through self-association of solute or solvent molecules via hydrophobic, dipole, van der Waals, and hydrogen interactions as well as Coulombic and hard-sphere repulsions.^{1,6–8} Moreover, the occurrence of LLPS is correlated with solvent polarity, molecular size, H-bonding character, cohesive energy density, solvent ratio, high electrolyte concentration, and differences in molecular weights between the solvents and the solutes.^{4,7,9,10}

The increase in approved hydrophobic drugs has correlated with the prevalence of LLPS. Hydrophilic molecules obtain anchoring sites and thus crystallize in a more organized and robust way from a solvent without undergoing LLPS. Hydro-

Received: February 28, 2022

Revised: August 29, 2022

Published: September 14, 2022



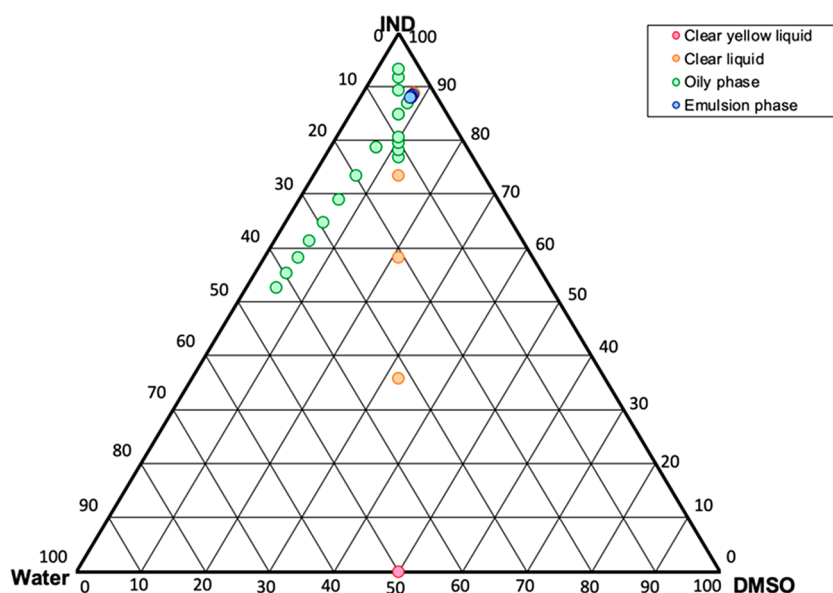


Figure 1. Phase diagram of IND in DMSO with water, showing changes in water/concentration that lead to visible changes and various phases at 25 °C.

phobic molecules with low polarities lack those anchoring sites and are therefore more prone to undergo LLPS.¹¹

There are various reported approaches to prevent LLPS. These include changing the processing parameters such as decreasing the solute concentration and altering solvents or temperature.⁴ Another reported method is the addition of a seed to encourage crystal growth.¹² Altering processing parameters to obtain solids can be difficult and time-consuming. Sophisticated tools have been used to tackle LLPS such as freeze-drying. A phase diagram provides an understanding of how a system behaves when subjected to different conditions, illustrating the different phases. Previously the effect of temperature and its induction of LLPS in protein solutions has been reported.¹³

We are reporting for the first time a method to recover and prevent the disposal of precious active materials via cocrystallization. Indomethacin (IND) was used as a model active material which tends to form LLPS with DMSO and water as a solvent and an antisolvent, respectively. Moreover, IND is known to form a 1:1 cocrystal with saccharin (SAC).

EXPERIMENTAL SECTION

Materials. Indomethacin (IND; purity 98%), saccharin (SAC; purity 98+%), and dimethyl sulfoxide (DMSO) were purchased from Alfa Aesar (U.K.).

LLPS Cocrystal Synthesis. A saturated IND solution was prepared by dissolving IND (1 g, 2.79 mmol) in dimethyl sulfoxide (3 mL). This resulted in a clear yellow solution, with a concentration of 286 mg mL⁻¹ (0.80 mmol mL⁻¹). Water (3 mL) was added to this solution, resulting in LLPS. The solution was in two distinct phases: a liquid phase (LP) and a highly viscous oily phase (OP). The solution was stirred, after which the LP was discarded leaving the OP, which was further rinsed with water (12 mL) to remove any residual LP. The OP had an IND concentration of 495 g g⁻¹, of which 723 mg (1 mmol) was taken to which an excess of SAC 366 mg (2 mmol) was added. The SAC was then stirred into the OP until it was fully dissolved and IND:SAC cocrystals were obtained. The resulting mixtures were monitored by *in situ* photoluminescence (PL), X-ray diffraction (XRD), and spectroscopy. A series of spectrograms were taken consecutively to monitor the growth of cocrystals.

Powder X-ray Diffraction (PXRD). X-ray diffraction patterns were recorded with a Bruker D8 Advance X-ray powder diffractometer with

Cu K α radiation of 1.5406 Å wavelength in the 2θ range between 5 and 50° 2θ in steps of 0.02° with a time count of 2 s in continuous scanning mode; the full scan took 490 s.

Rietveld refinement was carried out on the data collected at the different time points for saccharin cocrystal mixes with the use of GSAS-II. After an initial LeBail fit to optimize background, peak shape, and sample shift parameters, the crystal structures were refined as rigid bodies, with peak position, preferred orientation, and phase composition parameters varied as required.

Starting crystal models for each phase were obtained from the Cambridge Structural Database (REFCODES for saccharin, SCCHRN; for α -indomethacin, INDMET02; and for saccharin- α -indomethacin cocrystal, UFERED).

Photoluminescence Spectroscopy (PL). Excitation spectra were obtained with a FluoroMax-4 spectrofluorometer; the excitation wavelength was 300 nm. The gel-like samples were added into the solid sample holder, and an excitation spectrum was obtained every 2 min for 120 min. Liquid samples were placed in a cuvette which was then placed in the FluoroMax-4, and an excitation spectrum was obtained. All excitation spectra were obtained at an excitation wavelength of 300 nm, with entrance and exit slit spacings of 1 mm each. Data was analyzed with the use of the FluorEssence and Microsoft Excel software packages.

High-Performance Liquid Chromatography (HPLC). A Waters e-2695 system integrated with a photodiode array (PDA) detector 2998 was used to analyze the samples. Full experimental details are provided in the [Supporting Information](#).

Thermogravimetric Analysis (TGA). A Q5000 equipped with an RSC90 cooling unit by TA Instruments (Crawley, U.K.) was used in this study for decomposition analysis. Experimental samples used were 5 \pm 1 mg at a heating rate of 10 °C/min under a nitrogen gas flow at 25 mL/min with a temperature range of 25–600 °C. The results obtained from the TGA were analyzed with TA Universal Analysis software.

Differential Scanning Calorimetry (DSC). A Q2000 DSC equipped with an RSC90 cooling unit by TA Instruments (Crawley, U.K.) was used in this study to determine the thermal behavior of samples. The instrument was calibrated with indium metal. Experiments were carried out with samples of 1–4 mg of material in sealed aluminum pans. An empty sealed pan was used as a reference. Several different methods were used in different areas of this study, with the most common method being a ramp from 25 °C to 20 °C below the decomposition temperature of the sample at 10 °C/min. An inert atmosphere was maintained by purging with nitrogen at 50 mL/min.

The thermograms produced were analyzed with TA Universal Analysis software.

RESULTS AND DISCUSSION

In the attempt to obtain crystalline indomethacin (IND) by the antisolvent method, LLPS occurred, which slowed the process of solid production. The oily phase was then separated and observed under a microscope to determine how crystallization was taking place. It was observed that the oily phase was an emulsified state containing water, IND, and dimethyl sulfoxide (DMSO). Interfacial crystallization was observed at the oil–water boundary. To gain understanding, a phase diagram was produced (Figure 1); this was compiled by altering various processing parameters (the design of experiments is provided in the Supporting Information). Solutions of various concentrations were prepared by dissolving IND in 3 mL of DMSO and stirring them gently at 50 °C. These solutions were then taken, and the corresponding volume of water was added. The effect of IND concentration was determined by fixing solvent volumes while altering the mass of IND. The effect of solvent ratios was investigated by altering the volume of water while keeping the volume of the IND in the DMSO solution constant. There are four sections based on different appearances and features, as shown in Figure 1. The liquid samples were analyzed with HPLC to determine the concentration of IND. Furthermore, no additional peaks were detected after the oiling out, indicating that the sample did not undergo any degradation during processing. The raw data are provided in the Supporting Information.

The liquid phase was clear, whereas the emulsion phase was milky. The oily phase instantly settled to the bottom of the vessel as it was considerably viscous and its formation was highly distinctive. Vessels with oily phases always contained an emulsion phase at the top. In addition, the phase diagram illustrates how LLPS can be avoided, by using low concentrations of IND. The solubility of IND in DMSO at ambient temperature was determined by HPLC (the method is provided in the Supporting Information). The time taken for production of crystals after LLPS was considerably slower than that for those normally obtained by solvent antisolvent crystallization. As separation of solid from the oily phase is challenging and products must be obtained in a reasonable time, cocrystallization was attempted. This accelerated the production of crystals from the nucleating oily phase. Previously, cocrystallization has been used to stabilize liquids; however, this is the first report of exploiting cocrystallization to minimize drug losses due to LLPS, reducing waste and preventing disposal complexities arising, thus providing an economic benefit.^{14,15} The solute-rich oily phase is transformed to cocrystals by the addition of a suitable cofomer.

The method presented in this study allows the production of cocrystals by utilizing the oily phase formed due to LLPS.^{6,16} As cocrystallization from LLPS is not instantaneous, it was possible to monitor the progress of cocrystal formation *in situ*. IND cocrystals were not obtained by antisolvent cocrystallization due to the liquid–liquid phase separation (LLPS) phenomenon. Despite alteration of the processing parameters, cocrystals could not be obtained with the use of the solvents DMSO and water. The two phases were then separated, and the highly concentrated oily phase was used for cocrystallization. This provides a major advantage in producing cocrystals of molecules prone to LLPS without having to alter processing parameters.

Initially the system consisted of amorphous IND as shown in Figure 2A. Hump XRD diffractograms were obtained, without

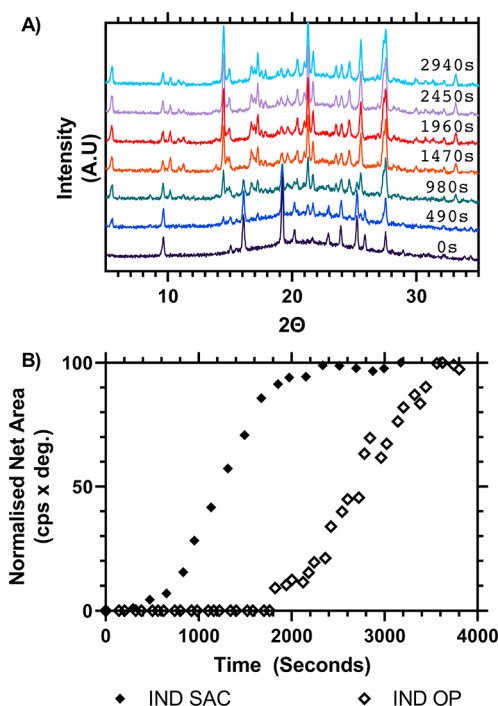


Figure 2. (A) Consecutive XRD diffractograms of IND oily phase mixed with SAC taken at intervals of 490 s (T1–T7, from bottom to top). Further time point diffractograms showing that there are no changes after T7 are provided in the Supporting Information. (B) Changes in net area of characteristic peaks for IND and IND:SAC.

any peaks characteristic of crystalline IND. Progressively the intensity at various 2θ values increased due to the onset of crystallization together with the baseline becoming smoother. The normalized net area of the characteristic peaks ($2\theta = 20.5^\circ$ for IND and $2\theta = 5.8^\circ$ for IND:SAC) was determined and plotted against time as shown in Figure 2B. The net area increased; this corresponds directly to the amount of crystalline material within the sample. Nucleation onset of the IND:SAC cocrystals was significantly faster than that of IND crystals. We suggest that the cofomer SAC is selectively forming hydrogen bonds with the API with higher affinity and hence at a higher rate.

Rietveld refinement was carried out to evaluate indomethacin–saccharin cocrystal growth and kinetics while accounting for the impacts of particle size, morphology, and any other phases that may occur. Results showed that initially the only crystalline component was SAC; gradually the cocrystal percentage increased with concurrent γ -IND formation. The formation of γ -IND occurred after T3 (see Figure 2A) compared to the IND:SAC cocrystal. This method also demonstrated the formation of α -IND (metastable form) at T5, after which its amount decreased possibly due to its greater tendency to form cocrystals. The time points T3–T6 showed an increase in γ -IND, after which it decreased due to an increase in cocrystals. Cocrystal formation is quicker than that of IND alone. We hypothesize that it is more thermodynamically favored. These trends concur with other analytical methods in this study. This Rietveld refinement is based upon relative amounts within the crystalline phases, disregarding any amorphous phase. There-

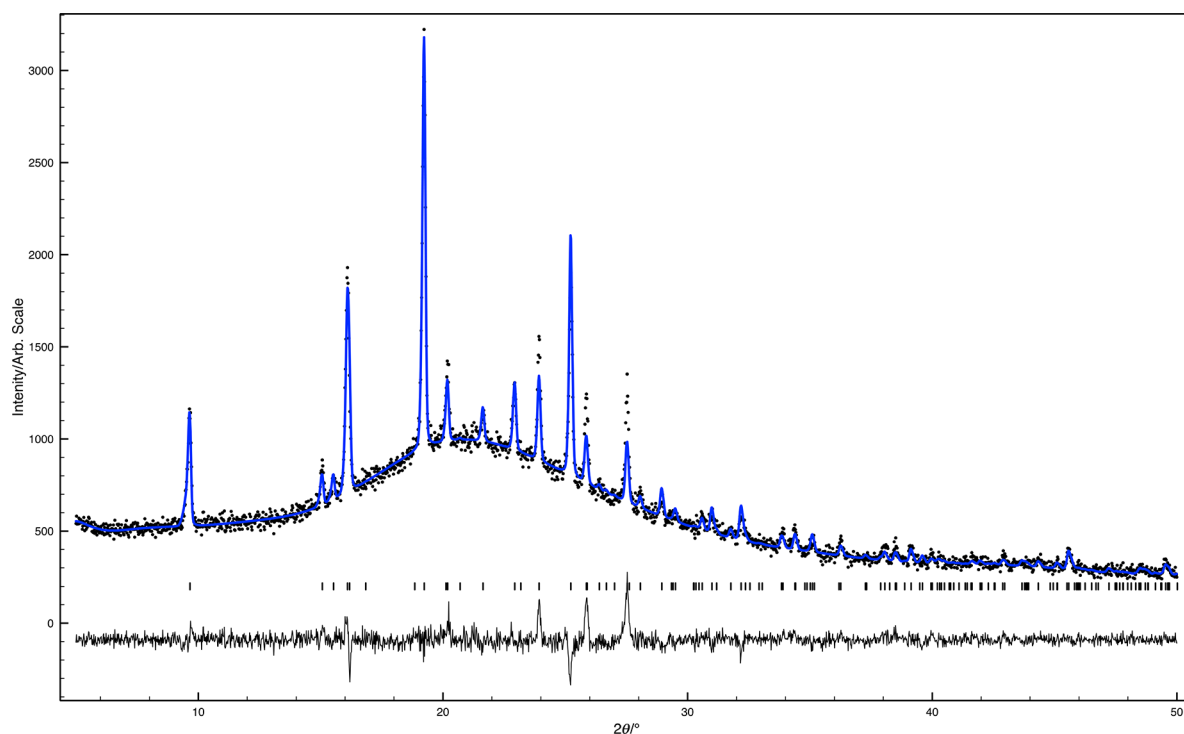


Figure 3. Final Rietveld fit (blue line) to collected T1 data (dots) with difference curve (black line). The reflection positions of saccharin (black) are shown as tick marks.

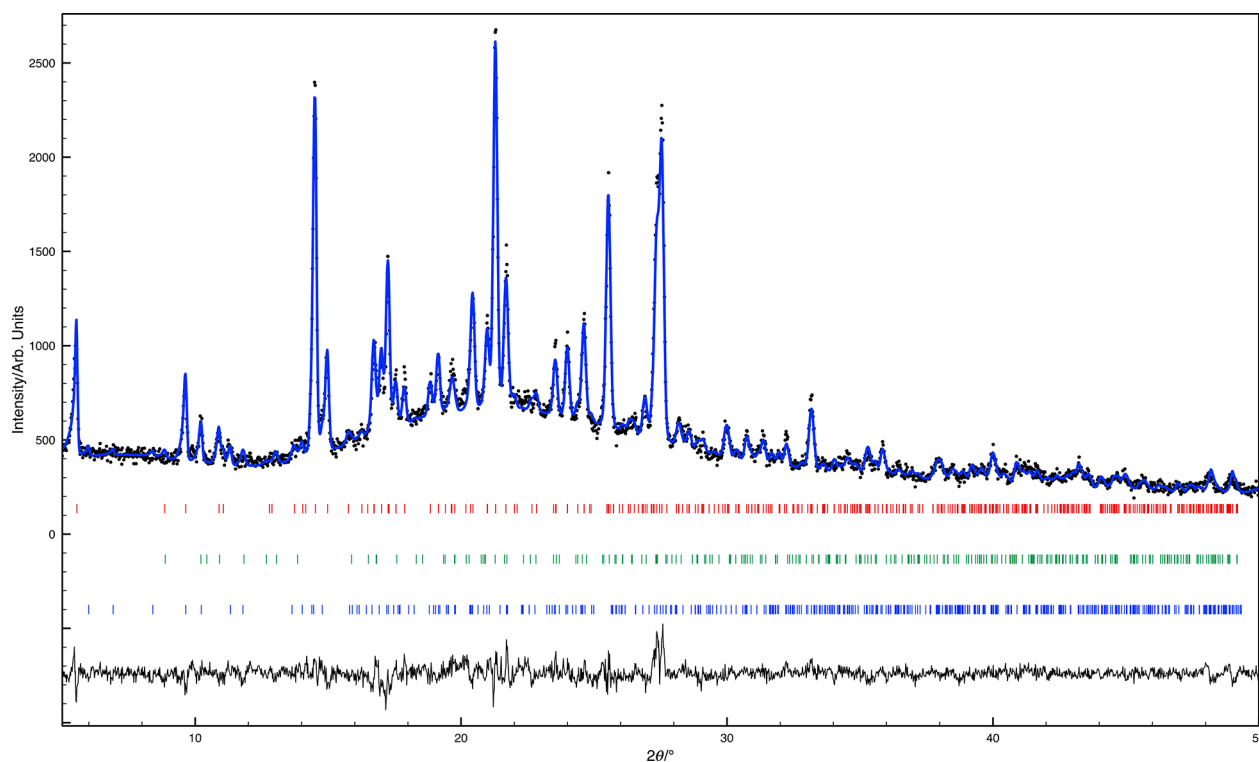


Figure 4. Final Rietveld fit (blue line) to collected T7 data (dots) with difference curve (black line). The reflection positions of the cocrystal (red), γ -indomethacin (green), and α -indomethacin (blue) phases are shown as tick marks.

fore, in the case of IND the result would always be 100% as there are no other crystal phases present.

Final plots of the Rietveld refinements are given in Figures 3 and 4 (first and last refinements carried out; all remaining plots have been included in the Supporting Information). Data sets

T8–T15 are the same as T7 and so were not refined since the ratios will be constant. The results as per Table 1 suggest that the sample had a yield of 92% cocrystals with the remainder as polymorphs of IND.

Table 1. Results of Rietveld Refinement

	$R_{wp}/\%$	% saccharin	% cocrystal	% γ -indomethacin	% α -indomethacin
T1	5.45	100	0	0	0
T2	5.33	57	43	0	0
T3	6.42	17	74	9	0
T4	7.31	4	90	6	0
T5	6.38	0	91	3	6
T6	6.18	0	84	12	4
T7	6.13	0	92	5	3

Thermal properties, behavior, and stability of the starting materials and cocrystals were studied by TGA and DSC, and thermographs are provided in the [Supporting Information](#). DSC analysis of the LLPS cocrystal indicated that the sample contained impurities due to a lower melting point (180.98 °C) compared to that formed via liquid assisted grinding (182.88 °C).

The feasibility of monitoring the reaction *in situ* by photoluminescence spectroscopy arose with significant changes in the PL spectra of IND alone and when mixed with the cofomer could be seen ([Figure 5B](#)) as crystallization

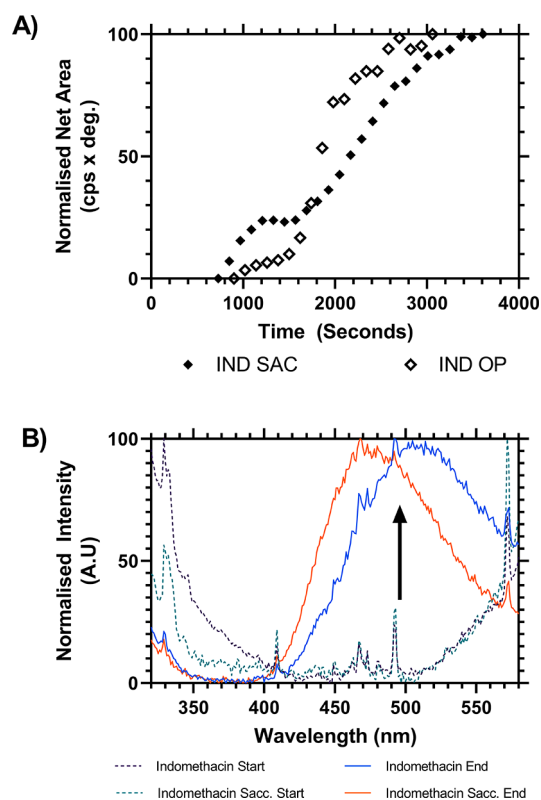


Figure 5. (A) Changes in photoluminescence intensity at 493 nm for IND:SAC and IND OP samples. (B) Photoluminescence excitation spectra captured at time 0 and after 60 min of IND oily phase with and without SAC.

progressed. In all cases several peaks transformed into one large hump due to the fluorescence properties of the crystalline molecules. The IND crystal molecules fluoresced continually from 424 nm substantially until over 576 nm, with maximum fluorescence intensity at 507 nm, whereas the IND:SAC cocrystal fluoresced continually from 458 nm substantially until over 576 nm, with maximum fluorescence at 470 nm. All spectra taken at the start were similar. Prior to crystallization, the

greatest fluorescence intensity occurred at lower wavelengths. Accordingly, the crystals had greater fluorescence intensity at higher wavelengths. Solid-state fluorescence has been previously used to distinguish amounts of amorphous and crystalline IND, as the intensity of the signal is proportional to sample crystallinity.¹⁷ An excitation wavelength of 300 nm was used, which is lower than that used in previous studies due to the higher mobility of the oily phase, particularly along the dihedral angle between the *p*-chlorophenyl moiety and the amide bond which can both extend and conjugate and provide a dissipative pathway.¹⁷ Despite the differences the general trend was the same: as the amount of amorphous IND was reduced, the intensity increased. The form changed the wavelength of maximum intensity in the study by Frenette et al.¹⁷ In the amorphous sample the maximum intensity was at 525 nm, whereas in the most stable γ -IND polymorph it was at 460 nm; i.e. the wavelength of maximum intensity decreased. However, in this study the wavelength increased as the sample became crystalline.

Crystallization of IND and that of IND:SAC after LLPS were observed at real time with the use of polarizing optical microscopy ([Figure 6](#)). The LLP was placed on a glass slide directly after the addition of water phase to the IND solution of DMSO. In the case of IND:SAC, SAC was added after water and then the OP was placed on the glass slide. Microscopic images show that crystallization of IND occurs at the LLPS interface. Moreover, the time required for crystallization was ca. 15 min and was completed after ca. 90 min. On the other hand, crystallization of IND:SAC was significantly more rapid compared to IND and started after ca. 3 min and was completed after 4 min. The crystallization took place mainly at the interface of LLPS, yet crystallization appeared on both oily and aqueous phases.

Crystallization kinetics of IND:SAC were measured by using Rietveld analysis to obtain an insight into the crystallization mechanism. IND crystallization kinetics were calculated based on the normalized net area of the characteristic peaks of γ -IND ($2\theta = 20.5^\circ$). Consequently, kinetics were analyzed using various mathematical models. Based on the mechanism, these models are classified as either nucleation and growth controlled, geometrical contractions, diffusion, or reaction order models ([Table 2](#)).

While the crystallization kinetics of IND are shown to be more fit to the 1D phase boundary model, the 3D diffusion or first order models are best fit for IND:SAC crystallization. In other words, the crystallization rate of IND is dependent on geometrical contraction models, which are based on the assumption that the nucleation process takes place instantaneously at the crystal surface or phase boundary. Therefore, the reaction is controlled by the formation of a new interface as the reaction proceeds.

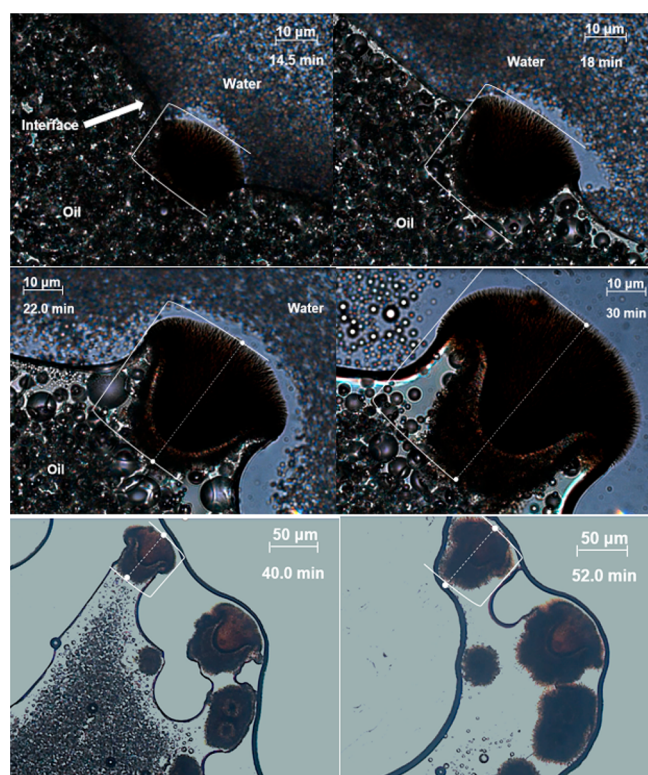


Figure 6. IND crystal growth during LLPS of water–DMSO. The growth takes place at the interface of the oil and water phases.

Table 2. Model Used in Fitting IND and IND:SAC Crystallization: Kinetic Models of IND Crystallization from the Oily Phase

model	abbreviation	integral function, $g(\alpha)$
Nucleation and Crystal Growth Models		
Prout–Tompkins	PT	$\ln[\alpha/(1-\alpha)] = kt$
Avrami–Erofeev ($n = 2$)	AE 2	$[-\ln(1-\alpha)]^{1/2} = kt$
Avrami–Erofeev ($n = 3$)	AE 3	$[-\ln(1-\alpha)]^{1/3} = kt$
Reaction Order Model		
first order	FO	$[-\ln(1-\alpha)] = kt$
Geometrical Contraction (Phase Boundary) Models		
one-dimensional	1D PB	$1 - \alpha = kt$
two-dimensional	2D PB	$1 - (1-\alpha)^{1/2} = kt$
three-dimensional	3D PB	$1 - (1-\alpha)^{1/3} = kt$
Diffusion Models		
one-dimensional	1D D	$\alpha^2 = kt$
two-dimensional	2D D	$(1-\alpha) \ln(1-\alpha) + \alpha = kt$
three-dimensional	3D D	$[1 - (1-\alpha)^{1/3}]^2 = kt$
Ginstling–Brounstein	GB	$1 - (2\alpha/3) - (1-\alpha)^{2/3} = kt$

On the other hand, the IND:SAC crystallization rate is dependent on either a 3D diffusion or first order model with r^2 values of 0.909 and 0.899, respectively (Table 3). Diffusion models propose that solid-state kinetics have a heterogeneous nature; i.e., the reactants remain, on the microscopic level, unevenly mixed during the reaction. Therefore, the reaction rate is controlled by the diffusion motion between the two solids. The first order model proposes that the reaction is homogeneous and the conversion is proportional to the reactant concentration. The change in crystallization rate dependency from geometrical contraction to diffusion or first order models

Table 3. Model Used in Fitting IND and IND:SAC Crystallization: Fit Parameters for the Kinetic Models of Crystallization from the Oily Phase

model	IND	IND:SAC
PT	0.8980	0.1272
AE 2	0.8544	0.7962
AE 3	0.9142	0.7071
FO	0.5995	0.8990
1D PB	0.9696	0.1422
2D PB	0.9235	0.8298
3D PB	0.8601	0.8558
1D D	0.9220	0.8341
2D D	0.8471	0.8709
3D D	0.5619	0.9092
GB	0.7745	0.8863

can aid in understanding why the crystallization rate has increased significantly in the case of IND:SAC.¹⁸

PL and XRD both exhibited significant changes in their spectra due to the gradual phase transformation from amorphous to crystalline. The onset of crystallization varied when it was analyzed with different techniques, which can be attributed to environmental factors such as temperature and operational variables.

CONCLUSION

LLPS cocrystallization is a technique to obtain cocrystals from LLPS, at which stage development would normally stop until experimental parameters prevented the formation of LLPS. The methods presented allowed us to determine when crystallization was complete together with confirmation of crystal/cocrystal polymorphs. In summary, we report a novel method of cocrystallization of molecules that undergo LLPS for which altering the processing method may not be suitable. IND was used as a model compound, and IND:SAC cocrystals were successfully obtained with this method. This provides a developmental pathway starting from LLPS and obtaining cocrystals that would be difficult to obtain by other means.

ASSOCIATED CONTENT

Supporting Information

The Supporting Information is available free of charge at <https://pubs.acs.org/doi/10.1021/acs.cgd.2c00263>.

HPLC method, design of experiments, XRD diffractograms, Rietveld refinement, thermograms (PDF)

AUTHOR INFORMATION

Corresponding Author

Anant Paradkar – Centre for Pharmaceutical Engineering Science, School of Pharmacy and Medical Sciences, University of Bradford, Bradford BD7 1DP, United Kingdom; orcid.org/0000-0003-1704-9858; Email: A.Paradkar1@bradford.ac.uk

Authors

M. Asim Sajid Al-Hanafi – Centre for Pharmaceutical Engineering Science, School of Pharmacy and Medical Sciences, University of Bradford, Bradford BD7 1DP, United Kingdom
Mhd Bashir Alsirawan – Centre for Pharmaceutical Engineering Science, School of Pharmacy and Medical Sciences, University of Bradford, Bradford BD7 1DP, United Kingdom; orcid.org/0000-0002-7998-5919

Colin C. Seaton – School of Chemistry and Biosciences, University of Bradford, Bradford BD7 1DP, United Kingdom; orcid.org/0000-0003-4094-720X

Thomas Swift – School of Chemistry and Biosciences, University of Bradford, Bradford BD7 1DP, United Kingdom; orcid.org/0000-0002-8616-8458

Sudhir Pagire – Centre for Pharmaceutical Engineering Science, School of Pharmacy and Medical Sciences, University of Bradford, Bradford BD7 1DP, United Kingdom

Venu R. Vangala – Centre for Pharmaceutical Engineering Science, School of Pharmacy and Medical Sciences, University of Bradford, Bradford BD7 1DP, United Kingdom; orcid.org/0000-0002-0836-2052

Adrian L. Kelly – Centre for Pharmaceutical Engineering Science, Faculty of Engineering and Informatics, University of Bradford, Bradford BD7 1DP, United Kingdom

Complete contact information is available at:
<https://pubs.acs.org/10.1021/acs.cgd.2c00263>

Author Contributions

The manuscript was written through contributions of all authors. All authors have given approval to the final version of the manuscript.

Notes

The authors declare no competing financial interest.

ABBREVIATIONS

API, active pharmaceutical ingredient; DMSO, dimethyl sulfoxide; IND, indomethacin; LLP, liquid–liquid phase; LLPS, liquid–liquid phase separation; PL, photoluminescence; SAC, saccharin; XRD, X-ray diffraction

REFERENCES

- (1) Sun, M.; Du, S.; Chen, M.; Rohani, S.; Zhang, H.; Liu, Y.; Sun, P.; Wang, Y.; Shi, P.; Xu, S.; et al. Oiling-Out Investigation and Morphology Control of β -Alanine Based on Ternary Phase Diagrams. *Cryst. Growth Des.* **2018**, *18* (2), 818–826.
- (2) Ceballos, A. V.; McDonald, C. J.; Elbaum-Garfinkle, S. Methods and Strategies to Quantify Phase Separation of Disordered Proteins. *Methods Enzymol.* **2018**, *611*, 31–50. Mosses, J.; Turton, D. A.; Lue, L.; Sefcik, J.; Wynne, K. Crystal templating through liquid–liquid phase separation. *Chem. Commun.* **2015**, *51* (6), 1139–1142. de Albuquerque, I.; Mazzotti, M. Influence of Liquid-Liquid Phase Separation on the Crystallization of L-Menthol from Water. *Chem. Eng. Technol.* **2017**, *40* (7), 1339–1346.
- (3) Paul, E. L.; Tung, H.-H.; Midler, M. Organic crystallization processes. *Powder Technol.* **2005**, *150* (2), 133–143. Kashchiev, D.; Van Rosmalen, G. M. Review: Nucleation in solutions revisited. *Crystallization Research and Technology* **2003**, *38* (7–8), 555–574. Variankaval, N.; Cote, A. S.; Doherty, M. F. From form to function: Crystallization of active pharmaceutical ingredients. *AIChE J.* **2008**, *54* (7), 1682–1688.
- (4) Lu, J.; Li, Y.-P.; Wang, J.; Ren, G.-B.; Rohani, S.; Ching, C.-B. Crystallization of an active pharmaceutical ingredient that oils out. *Sep. Purif. Technol.* **2012**, *96*, 1–6.
- (5) Veessler, S.; Revalor, E.; Bottini, O.; Hoff, C. Crystallization in the presence of a liquid–liquid phase separation. *Org. Process Res. Dev.* **2006**, *10* (4), 841–845.
- (6) Duffy, D.; Cremin, N.; Napier, M.; Robinson, S.; Barrett, M.; Hao, H.; Glennon, B. In situ monitoring, control and optimization of a liquid–liquid phase separation crystallization. *Chem. Eng. Sci.* **2012**, *77*, 112–121.
- (7) Derdour, L. A method to crystallize substances that oil out. *Chem. Eng. Res. Des.* **2010**, *88* (9), 1174–1181.
- (8) Deneau, E.; Steele, G. An In-Line Study of Oiling Out and Crystallization. *Org. Process Res. Dev.* **2005**, *9* (6), 943–950.
- (9) Du, Y.; Wang, H.; Du, S.; Wang, Y.; Huang, C.; Qin, Y.; Gong, J. The liquid–liquid phase separation and crystallization of vanillin in 1-propanol/water solution. *Fluid Phase Equilib.* **2016**, *409*, 84–91.
- (10) Wada, S.; Kudo, S.; Takiyama, H. Development of simultaneous control of polymorphism and morphology in indomethacin crystallization. *J. Cryst. Growth* **2016**, *435*, 37–41.
- (11) *Handbook of Pharmaceutical Salts: Properties, Selection, and Use*; Stahl, P. H., Wermuth, C. G., Eds.; Verlag Helvetica Chimica Acta: Zürich, Switzerland, and Wiley-VCH: Weinheim, Germany, 2002.
- (12) Patience, D. B.; Dell’Orco, P. C.; Rawlings, J. B. Optimal Operation of a Seeded Pharmaceutical Crystallization with Growth-Dependent Dispersion. *Org. Process Res. Dev.* **2004**, *8* (4), 609–615.
- (13) McCarty, J.; Delaney, K. T.; Danielsen, S. P. O.; Fredrickson, G. H.; Shea, J.-E. Complete Phase Diagram for Liquid–Liquid Phase Separation of Intrinsically Disordered Proteins. *J. Phys. Chem. Lett.* **2019**, *10* (8), 1644–1652.
- (14) Bacchi, A.; Mazzeo, P. P. Cocrystallization as a tool to stabilize liquid active ingredients. *Crystallography Reviews* **2021**, *27* (2), 102–123.
- (15) Liu, L.; Wang, J.-R.; Mei, X. Enhancing the stability of active pharmaceutical ingredients by the cocrystal strategy. *CrystEngComm* **2022**, *24* (11), 2002–2022.
- (16) Parimaladevi, P.; Supriya, S.; Srinivasan, K. The role of ultrasound in controlling the liquid–liquid phase separation and nucleation of vanillin polymorphs I and II. *J. Cryst. Growth* **2018**, *484*, 21–30.
- (17) Frenette, M.; Cosa, G.; Friščić, T. Characterisation of organic solid forms and real-time in situ monitoring of their transformations using solid-state fluorescence. *CrystEngComm* **2013**, *15* (25), 5100–5106.
- (18) Khawam, A.; Flanagan, D. R. Solid-State Kinetic Models: Basics and Mathematical Fundamentals. *J. Phys. Chem. B* **2006**, *110* (35), 17315–17328.

Recommended by ACS

Use of Wet Milling Combined with Temperature Cycling to Minimize Crystal Agglomeration in a Sequential Antisolvent–Cooling Crystallization

Zhuang Sun, Chris D. Rielly, et al.

JULY 19, 2022
CRYSTAL GROWTH & DESIGN

READ 

Gas-Assisted Cocrystal Desublimation

Shea Sanvordenker, Max Shtein, et al.

FEBRUARY 04, 2022
CRYSTAL GROWTH & DESIGN

READ 

Continuous Antisolvent Crystallization of Dolutegravir Sodium Using Microfluidics

Fen Liu, Bo Bao, et al.

MAY 06, 2022
INDUSTRIAL & ENGINEERING CHEMISTRY RESEARCH

READ 

Combining Viedma Ripening and Temperature Cycling Deracemization

Giuseppe Belletti, Elias Vlieg, et al.

JANUARY 31, 2022
CRYSTAL GROWTH & DESIGN

READ 

Get More Suggestions >